Front. Phys. 13(1), 134201 (2018)
DOI 10.1007/s11467-017-0707-5

RESEARCH ARTICLE

# Evolution of finite energy Airy beams in cubic-quintic atomic vapor system

**Zhen-Kun Wu[1], Hao Guo[1], Wei Wang[2†], Yu-Zong Gu[1‡]**

[1] *Institute of Microsystem Physics, School of Physics and Electronics, Henan University, Kaifeng 475004, China*
[2] *Key Laboratory for Physical Electronics and Devices of the Ministry of Education, The School of Electronic and Information Engineering, Xi'an Jiaotong University, Xi'an 710049, China*
*Corresponding author. E-mail: †wei_wang2014@mail.xjtu.edu.cn; ‡yzgu@henu.edu.cn*
*Received May 2, 2017; accepted June 23, 2017*

In a numerical investigation, we demonstrate the evolution of a one-dimensional and two-dimensional finite energy Airy beam in a Λ-type three-level atomic vapor with linear, cubic, and quintic susceptibilities considered simultaneously with the dressing effect. Quasi-solitons and soliton pairs are observed due to this competition mechanism. We find that the frequency detuning of the pump field and its power greatly affect the formation and evolution of generated solitons. In general, around the two-photon resonance point and for low intensities of the pump field, it is less difficult to form solitons. This investigation enriches the study of the propagation properties of Airy beams and soliton generation in atomic vapor.

**Keywords** airy beam, cubic-quintic nonlinear, soliton, atomic vapor system

**PACS numbers** 03.65.Ge, 03.65.Sq, 42.25.Gy



## 1 Introduction

Due to the remarkable and interesting properties including transverse acceleration [1], self-healing [2], and nondiffraction over many Rayleigh lengths [3], investigations on Airy beams have been abundant and have undergone rapid development over the past decade. They were first theoretically discovered by Berry and Balazs in 1979 [4]. Later, in 2007, the paraxial accelerating Airy beam was experimentally observed by Siviloglou and Christodoulides [2, 3]. Recently, the propagation dynamics of Airy beams have been studied extensively in nonlinear (NL) media. As an important optical NL effect, Zhang *et al.* have investigated the interactions of two in-phase and out-of-phase Airy beams in Kerr and saturable NL media [5, 6]. In these interactions, the bound and unbound soliton pairs, as well as single solitons, can be formed during propagation. Chen *et al.* have studied the effect of Kerr nonlinearity on an Airy-Gaussian beam [7]. It was demonstrated that their self-acceleration effect can be affected by the distribution factor. Moreover, further research along similar lines has been conducted by Chen *et al.* [8].

To overcome large absorption in atomic vapors, an electromagnetically induced transparency (EIT) window was developed. It is now broadly used in the propagation investigation of Airy beams in this medium. For instance, Zhuang *et al.* [9] as well as Hang and Huang [10] individually studied the propagation of Airy beams in EIT atomic vapor based on an open EIT system. Ye and Li theoretically studied the propagation of Airy beams in a close-Λ EIT system [11], in which the susceptibility and refractive index of the medium are calculated and analyzed. The pioneering studies on the NL propagation of Airy beams are only limited to the linear and cubic nonlinearity case, which can lead to a catastrophic self-focusing effect. However, previous investigations have revealed that the effect of quintic nonlinearity becomes significant and considerably influences optical soliton propagation at relatively high beam intensities [12–14]. Furthermore, quintic nonlinearity has been proposed to overcome the instability of multi-dimensional spatial solitons induced by cubic solitons [15, 16]. In this case, the focusing cubic and defocusing quintic NL effects should be considered simultaneously, i.e., NL propagation is determined by competing cubic-quintic (CQ) nonlinearities. To our knowledge, in the coherent atomic medium, we have not seen reports on the propagation dynamics of Airy beams in the case of quintic nonlin-

earity. Thus, the purpose of this work is to numerically study and analyze the evolution dynamics of a finite energy Airy beam under competition between third-order and fifth-order NL susceptibilities. Due to the multiparameter controllable properties of a multilevel atomic system, our research may broaden the field of the potential applications of Airy beams in atomic vapors.

## 2 Basic theory

The relevant energy levels for our scheme are shown in Fig. 1(a). The levels $|1\rangle$, $|2\rangle$, and $|3\rangle$ form a close-$\Lambda$ three-level atomic system. The probing beam $E_p$ (the wavevector $\boldsymbol{k}_p$ and frequency $\omega_p$) connects the transition $|1\rangle$ to $|2\rangle$ with the atomic resonant frequency $\omega_{21}$. The coupling beam $E_c$ ($\boldsymbol{k}_c$ and $\omega_c$), characterized by the resonant frequency $\omega_{23}$, drives the transition $|2\rangle$ to $|3\rangle$. We define the frequency detuning as $\Delta_p = \omega_{21} - \omega_p$ and $\Delta_c = \omega_{23} - \omega_c$, respectively. This is a typical $\Lambda$-type three-level atomic system and has been intensively studied. In our investigation, we show that this system can be used to theoretically study the propagation of a finite energy Airy beam. Its intensity profile is shown in Fig. 1(b), where the bottom insets present the intensity distribution of the Airy beam at $z = 0$ and $a$ is the decay factor that ensures the finite power of the Airy beam. In accordance with previous literatures [5, 6], we set the parameter $a = 0.1$ throughout this paper.

A general dimensionless form of the CQ NL Schrödinger equation (NLSE) can be written as

$$2\mathrm{i}k\frac{\partial\psi}{\partial Z} + \frac{\partial^2\psi}{\partial X^2} + k^2\chi\psi = 0, \tag{1}$$

where the spatially dependent function $\psi$ is the envelope of the modulated waves. The first term describes the longitudinal propagation, and the second term accounts for transverse diffraction with only the $X$-direction considered for mathematical simplicity. $X = x/w_0$, where $w_0$ is an arbitrary scaling parameter, $Z = z/Z_R$ is the normalized propagation distance, where $Z_R = kw_0^2$ is the Rayleigh length, and $k = 2\pi/\lambda$ is the wave number ($\lambda = \lambda_0$, where $\lambda_0$ is the vacuum wavelength). $\chi$ is the total susceptibility of the atomic vapor system, in which the involved linear, third-order, and fifth-order NL susceptibilities are respectively given as [17]

$$\chi^{(1)} = \frac{\eta}{K}, \tag{2a}$$

$$\chi^{(3)}|E_c|^2 = -\frac{\eta}{K^2}\frac{|\Omega_c|^2}{d_3}, \tag{2b}$$

$$\chi^{(5)}|E_c|^4 = -\frac{\eta}{K^3}\frac{|\Omega_c|^4}{d_3^2}, \tag{2c}$$

with $\eta = \mathrm{i}N\mu_{21}^2/(\hbar\varepsilon_0)$, $K = d_1 + |\Omega_c|^2/d_2 + |\Omega_p|^2/\Gamma_{11}$, $d_1 = \Gamma_{21} + \mathrm{i}\Delta_p$, $d_2 = \Gamma_{31} + \mathrm{i}(\Delta_p - \Delta_c)$, and $d_3 = \Gamma_{31} + \mathrm{i}(\Delta_p - \Delta_c) + |\Omega_p|^2/(\Gamma_{32} - \mathrm{i}\Delta_c)$, where $\Gamma_{ij}$ is the transverse relaxation rate between the states $|i\rangle$ and $|j\rangle$. $\Omega_p$ and $\Omega_c$ individually represent the Rabi frequencies of laser fields $E_p$ and $E_c$ with $\Omega_p = \mu_{12}E_p/\hbar$ and $\Omega_c = \mu_{23}E_c/\hbar$, where $\mu_{12}$ and $\mu_{23}$ are the electric dipole moments, and $N$is the atomic density. Combining Eqs. (2a)–(2c), we obtain the total susceptibility

$$\chi = \chi^{(1)} + \chi^{(3)}|E_c|^2 + \chi^{(5)}|E_c|^4, \tag{3}$$

The second and third terms in $\chi$ represent the cubic and quintic contributions to the total susceptibility. In Appendices A and B, we briefly present the derivation of

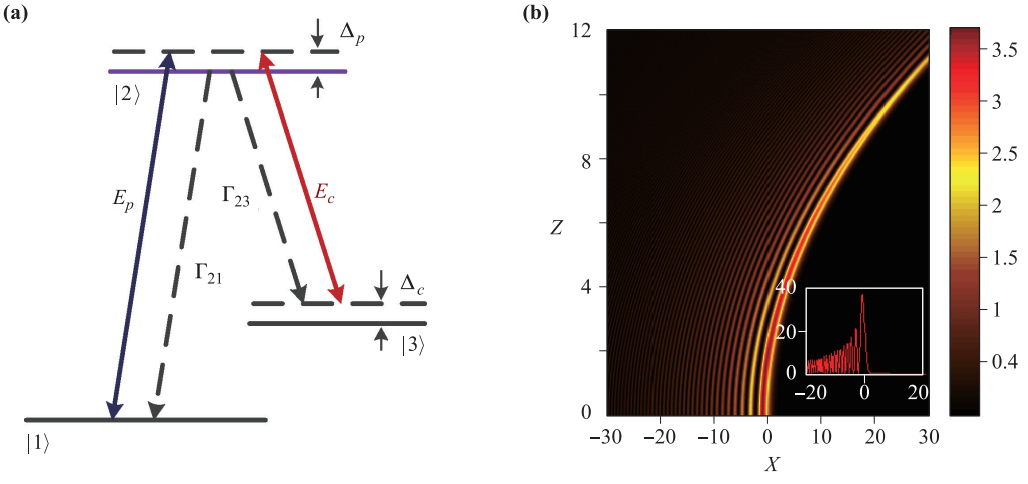


**Fig. 1** **(a)** Schematic of the atomic system. Probe and control fields are denoted as $E_p$ and $E_c$ individually, and these two fields are coupled with the atomic levels as shown above. **(b)** The spatial distribution of the Airy beam $\psi(x, z) = Ai(x - z^2/4 + iaz)\exp[i(6a^2z - 12iaz + 6iaz^2 + 6xz - z^3)/12]$ with parameter $a = 0.1$.

this susceptibility. In Eq. (3), $\Delta_p - \Delta_c = 0$ corresponds to the two-photon resonance condition that causes EIT [18]. It is worth mentioning that the probe field absorption is significantly decreased to seemingly zero in the EIT window.

Figure 2(a) depicts the theoretical NL susceptibility of the system versus $\Delta_c$ and the coupling intensity $\Omega_c$. The third-order and fifth-order dependencies of the real and imaginary parts of the linear term for $\Omega_c$ are presented in Figs. 2(b) and (c), respectively. The focusing and defocusing nonlinearities, which are respectively determined by the real parts of third-order and fifth-order susceptibilities, follow cubic-and quintic-dependent laws, but the former case is positive and the latter case is negative. As shown in Fig. 2(b), it is clear that the linear susceptibility is constant when varying $\Omega_c$. However, due to CQ nonlinearities, the real part of the total NL susceptibility experiences competition, which increases with $\Omega_c$ due to the dominant positive third-order nonlinearity increasing with a cubic law. However, as $\Omega_c$ exceeds a threshold value and reaches the high-power region, it begins to decrease because the negative fifth-order nonlinearity plays a dominant role on $\chi$. Figure 2(c) indicates the existence of this competition among both the real and imaginary parts of the third-order and fifth-order nonlinearities. Figure 2(a) also indicates that the competition between different nonlinearities can be controlled by both the coupling field detuning, $\Delta_c$, and $\Omega_c$.

## 3 Calculations and discussion

To explore the propagation properties of a finite energy Airy beam with competing CQ nonlinearities, we perform a numerical propagation calculation by employing the split-step fast Fourier transform (FFT) method. We choose $\psi(x,0) = \mathrm{Ai}(x)\exp(ax)$ as the incidence to execute the simulation for different $\chi$ parameters; intensity distributions are shown in Fig. 3 in which cubic and quintic nonlinearity is controlled by the adjustment of detuning $\Delta_c$ and power $\Omega_c$. First, we fixed $\Omega_c$ while adjusting $\Delta_c$. With the values $\Delta_c = -8\times10^{-6}\gamma_1$, $-4\times10^{-6}\gamma_1$, $-0.8\times10^{-6}\gamma_1$, and $-0.08\times10^{-6}\gamma_1$, the corresponding behaviors respectively shown in Figs. 3(a)–(d) are similar. The intensity distribution is fragmented as the main lobes and most of the side lobes of the Airy beam conserved their unique self-bent or self-acceleration properties in the horizontal axis $x$, an intense quasi-soliton pulse appeared near the beam center, and a very weak dispersion wave generated in the leading edge. The major difference is that, with a reduced $\Delta_c$, the energy is mainly stored to form a relatively strong central lobe during propagation whereas the side lobes become weaker and remain in their original position. When the relative detuning $\Delta_c$ is further reduced to $\Delta_c = 0$, $1.6\times10^{-9}\gamma_1$, and $2.4\times10^{-9}\gamma_1$, as shown in Figs. 3(e), (f), and (g), respectively, more energy flows to the central soliton pulse and becomes compressed, and breathing solitons are formed with specific periods. From these intensity images, it is evident that with reduced detuning $\Delta_c$ comes an increase in energy of the breathing system and a decrease in period of soliton breathing. Also visible is that the Airy wavepacket only remains with a very weak background, and it even collapses and quickly disappears. A comparison of Figs. 3(a)–(d) indicates that a difference in the detuning $\Delta_c$ can considerably affect the propagation evolutions. The essential reason for these exhibiting properties is the competition between third-order and fifth-order nonlinearities. From Eq. (3), we

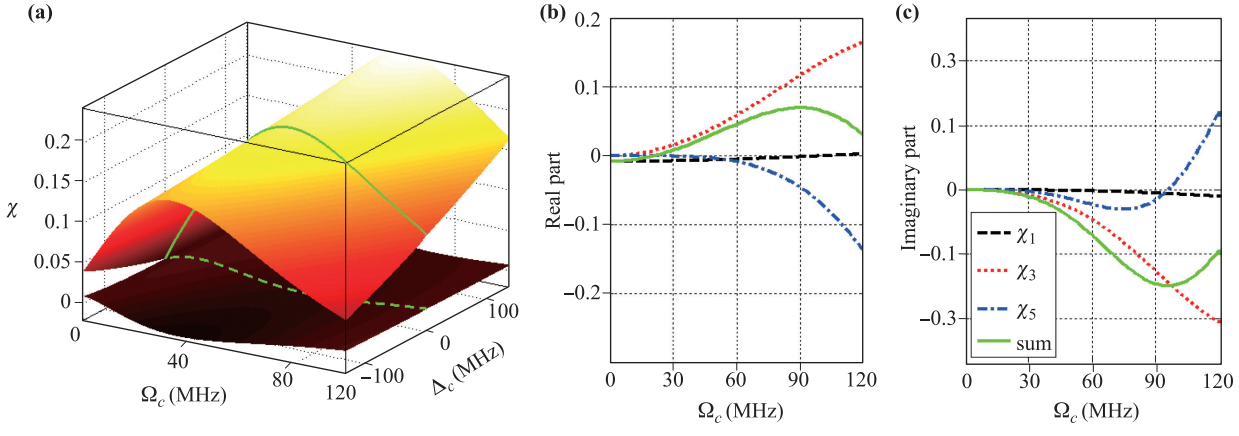


**Fig. 2** **(a)** Theoretical total susceptibility of the atomic vapor system as a function of $\Delta_c$ and $\Omega_c$. The top panel represents the real part; the bottom panel represents the imaginary part. The theoretically calculated real **(b)** and imaginary **(c)** parts of $\chi^{(1)}$, $\chi^{(3)}|E_c|^2$, $\chi^{(5)}|E_c|^4$, and their sum versus $\Omega_c$.

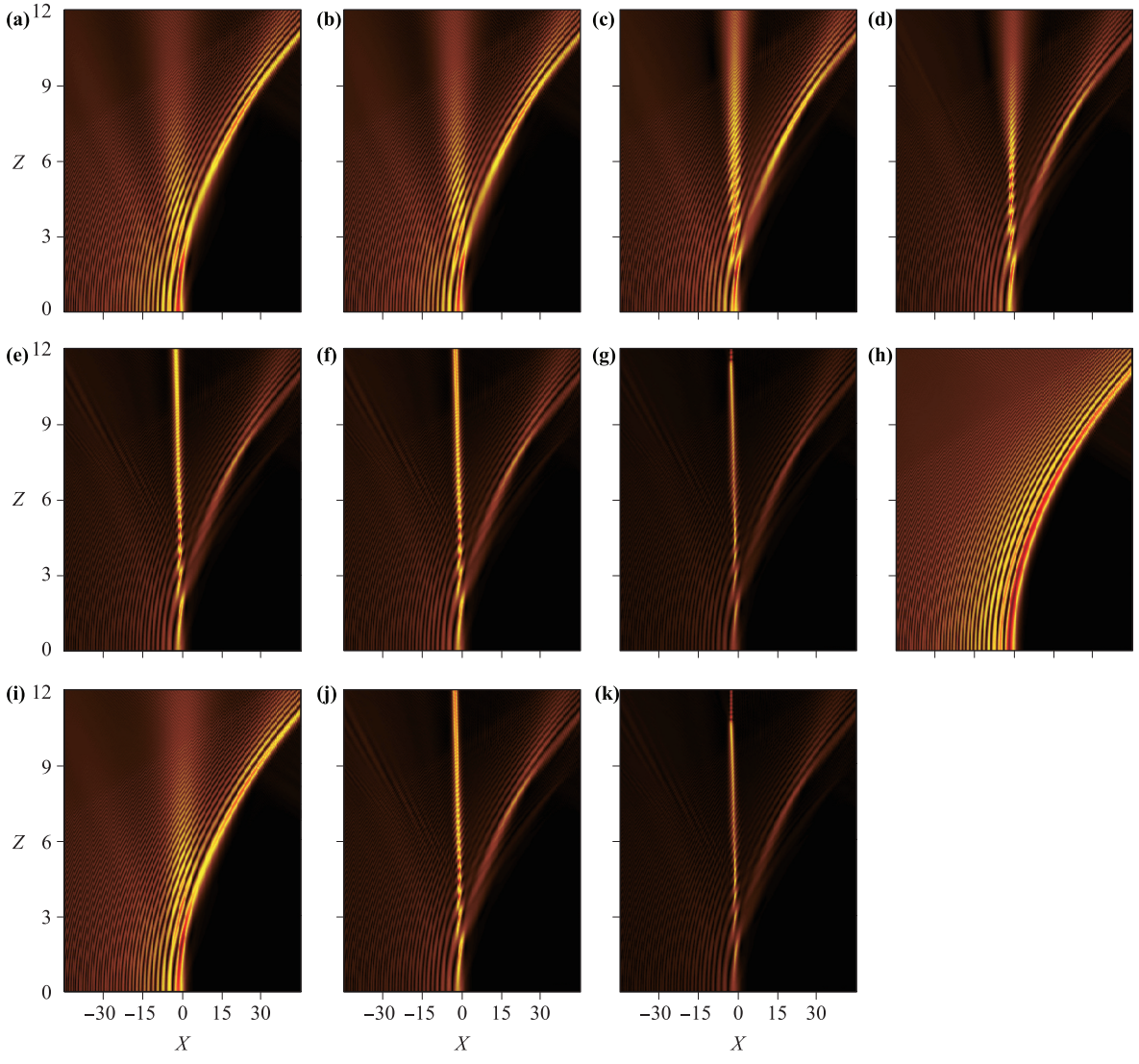


**Fig. 3** Propagation of the finite energy Airy beam in the atomic system for different values of $\Delta_c$ **(a–g)** and $\Omega_c$ **(h–k)**: with $\Delta_p = 0$ and $\Omega_c = 1.6\gamma_1$ (a) $\Delta_c = -8\times10^{-6}\gamma_1$, (b) $\Delta_c = -4\times10^{-6}\gamma_1$, (c) $\Delta_c = -0.8\times10^{-6}\gamma_1$, (d) $\Delta_c = -0.08\times10^{-6}\gamma_1$, (e) $\Delta_c = 0$, (f) $\Delta_c = 1.6\times10^{-9}\gamma_1$, and (g) $\Delta_c = 2.4\times10^{-9}\gamma_1$ and with $\Delta_p = \Delta_c = 0$ (h) $\Omega_c = 3\gamma_1$, (i) $\Omega_c = 2.5\gamma_1$, (j) $\Omega_c = 2\gamma_1$, and (k) $\Omega_c = 1.5\gamma_1$. The other parameters are $\Gamma_{21} = \gamma_1 + \gamma_2$, $\Gamma_{11} = \gamma_1/2$, $\Gamma_{32} = 2\gamma_2$, $\Gamma_{31} = \Gamma_{21}$, $\gamma_1 = 38$ MHz, $\gamma_2 = 10^{-3}\gamma_1$, and $\gamma_3 = \gamma_2$.

can find that the effect of $\Delta_c$ on the beam profile is reflected by the terms $\Gamma_{31} + \mathrm{i}(\Delta_p - \Delta_c)$ and $\Gamma_{32} - \mathrm{i}\Delta_c$ in the denominator, and it is negative causing the total NL susceptibility $\chi$ to increase with the decreasing process of $\Delta_c$. It can be predicted that a smaller frequency detuning $\Delta_c$ allows solitons to be more easily formed.

Next, we perform numerical simulations with a variable power $\Omega_c$. Figures 3(h)–(k) show a comparison of Airy beams for different $\Omega_c$ parameters, and they behave similar to those in Figs. 3(a)–(k). As shown in Figs. 3(h)–(k), an increased energy participates in the formation of bound breathing solitons during propagation with a decrease in $\Omega_c$. With a decrease in power, there is a decrease in the breathing soliton period. These features can also be attributed to competing CQ nonlinearities. The detailed explanations are similar to those used for Figs. 3(a)–(k).

To observe the propagation characteristics of an Airy beam in more detail, we extend the analysis to the two-dimensional (2D) case. Figure 4 show the corresponding peak intensity distributions at certain propagation distances for various $\Delta_c$ parameters. It is immediately visible that with an increase in propagation distance, the high frequency oscillation side lobes on the leading edge

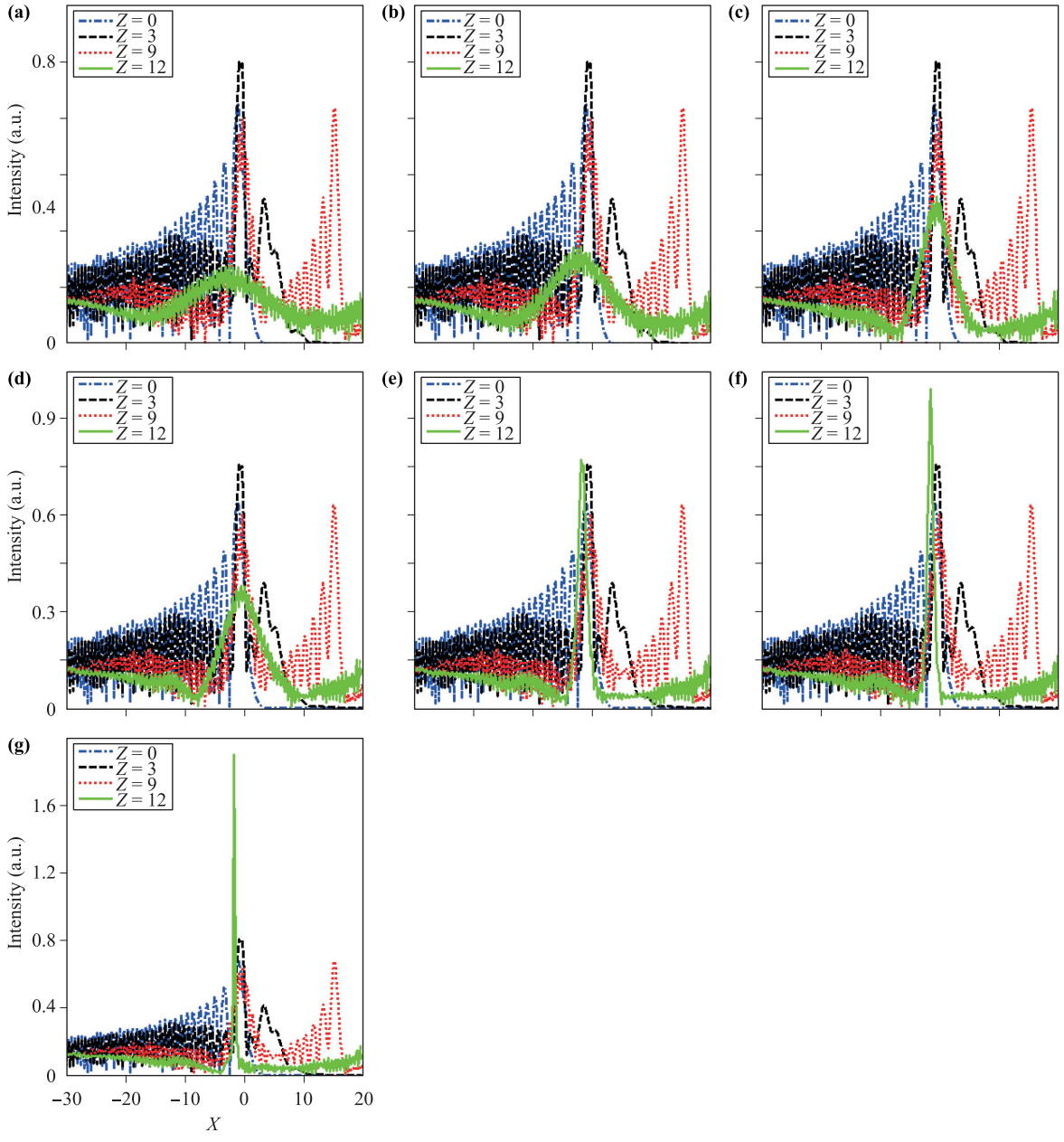


**Fig. 4** Two-dimensional evolution of finite energy Airy beam for different values of $\Delta_c$ with $\Delta_p = 0$ and $\Omega_c = 1.6\gamma_1$ **(a)** $\Delta_c = -8 \times 10^{-6}\gamma_1$, **(b)** $\Delta_c = -4 \times 10^{-6}\gamma_1$, **(c)** $\Delta_c = -0.8 \times 10^{-6}\gamma_1$, **(d)** $\Delta_c = -0.08 \times 10^{-6}\gamma_1$, **(e)** $\Delta_c = 0$, **(f)** $\Delta_c = 1.6 \times 10^{-9}\gamma_1$, and **(g)** $\Delta_c = 2.4 \times 10^{-9}\gamma_1$. The other parameters are $\Gamma_{21} = \gamma_1 + \gamma_2$, $\Gamma_{11} = \gamma_1/2$, $\Gamma_{32} = 2\gamma_2$, $\Gamma_{31} = \Gamma_{21}$, $\gamma_1 = 38$ MHz, $\gamma_2 = 10^{-3}\gamma_1$, and $\gamma_3 = \gamma_2$.

of the Airy beam and disappears gradually, and the leading edge will then become smooth. Only a minority of the side lobes remain. Moreover, the wave shape will shift towards the trailing edge of the Airy wavepacket. With a decreasing $\Delta_c$, the central intense soliton and the weak dispersion wave pulses shed from the Airy wavepackets will gradually emerge, as mentioned above. Notably, we can find that the beam width and oscillation intensity in the generated soliton decrease. This indicates that the stability of the Airy soliton is improved with a decrease in $\Delta_c$. CQ nonlinearities caused pulse compression, and an increase in dispersion wave pulse number can again be seen here.

In addition to the inputs with separable variables, one can also treat two-dimensional inputs with non-separable variables, e.g., an in circular finite-energy Airy beam [19].

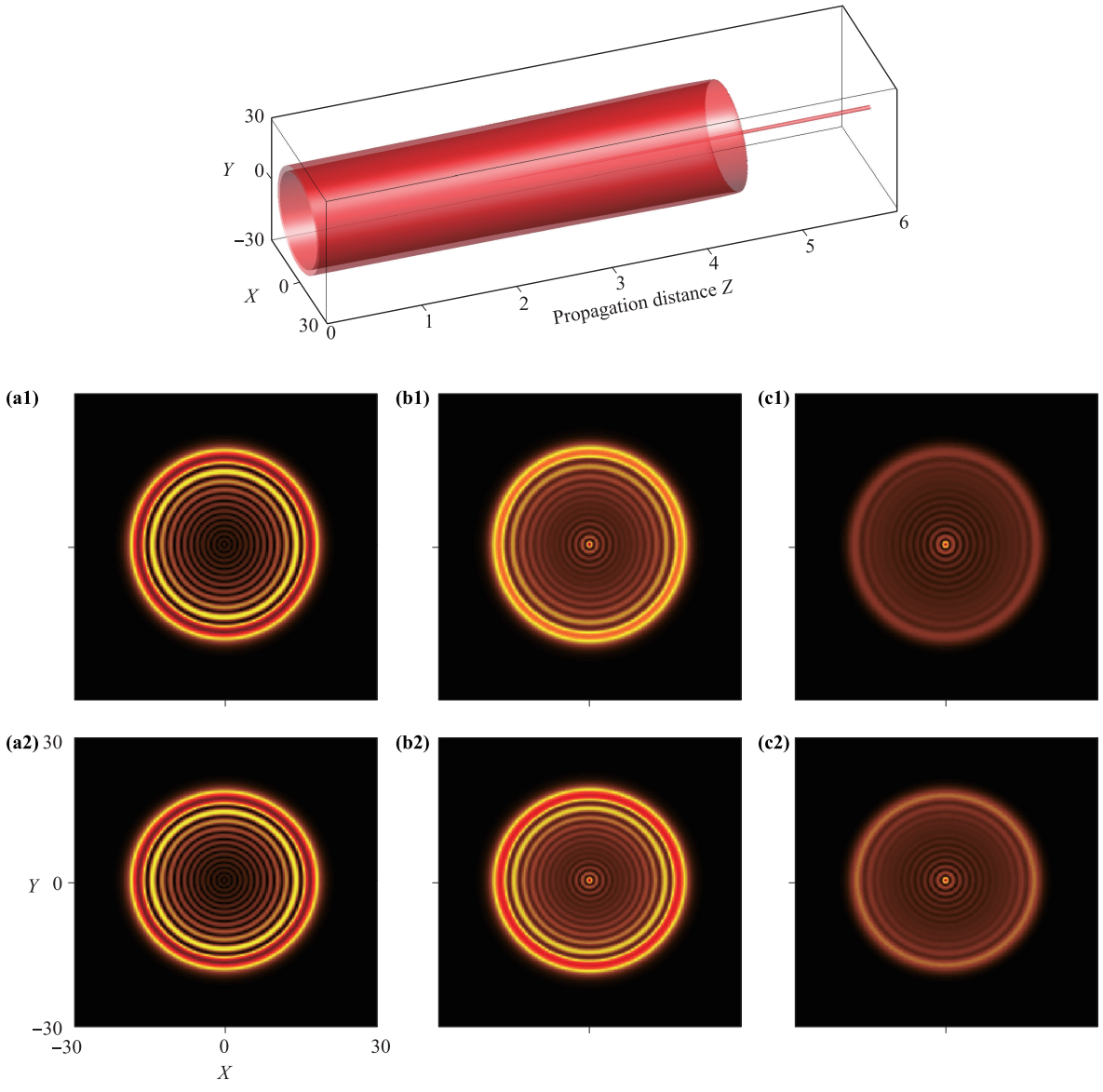


**Fig. 5** Propagation of two-dimensional a circular finite-energy Airy beam $\psi(X, Y, Z = 0) = \mathrm{Ai}(r - r_0)\exp[a(r - r_0)]$. With $\Delta_p = \Delta_c = 0$, isosurface plot of the intensity during propagation. (a1), (b1), and (c1) Intensity distribution when the beam propagates to $Z = 0$, $Z = 1.8$, and $Z = 3.6$, respectively. (a2), (b2), and (c2) setups are the same as those of (a1), (b1), and (c1), respectively, except for $\Delta_p = 0$ and $\Delta_c = -4 \times 10^{-6}\gamma_1$. The other parameters are $a = 0.1$ and $r_0 = 10$.

This type of initial beam can be written in polar coordinates as

$$\psi(X, Y, Z = 0) = \mathrm{Ai}(r - r_0)\exp[a(r - r_0)], \tag{4}$$

where $\mathrm{Ai}(r)$ represents airy function, $r_0$ is the mean radius and determines the location of the main ring. We first display the isosurface plot of the in circular Airy (CAi) beam during propagation in the top panel of Fig. 5. It can be clearly seen that CQ cannot support the stable propagation of the Airy beam, and the profile of which undergoes a profound change and transforms into a soliton profile. To elucidate propagation, we also present beam intensities obtained numerically at certain distances, as displayed in Figs. 5(a1)–(c1). We note here that Figs. 5(a1)–(c1) are obtained in the same scale. Comparing Fig. 5(a1) with Fig. 5(b1), the size of the ring of the CAi beam remains the same during propagation while the transverse intensities redistribute. Notably, the soliton is formed around the origin in this process. When the beam further propagates to $Z \approx 3.6$, the Airy profile dims and undergoes curious shape change

as displayed in Fig. 5(c1) in which the central soliton accumulates the most energy and becomes more robust. If we set the $\Delta_c = -4 \times 10^{-6}\gamma_1$ and redo the simulation. The corresponding evolutions of the 2D Airy beam are displayed in Figs. 5(a2), (b2), and (c2), where in this case, less energy distributes to form a central soliton than for $\Delta_c = 0$. This is because the competing CQ nonlinearities play an important role in the evolution, which has been explicated in Fig. 3.

## 4 Conclusion

In summary, we numerically investigated the evolution of one-dimensional and two-dimensional finite energy Airy beams in atomic vapor under CQ competing nonlinearity enhanced by EIT. The appearance of breathing solitons results from a competition between the third-order and fifth-order NL susceptibilities, which is greatly affected by the detuning, $\Delta_c$, and the power, $\Omega_c$. In general, the smaller the values for $\Delta_c$ and $\Omega_c$, the more significant energy is obtained in the breathing system, and the smaller the period of soliton breathing. Under this competition mechanism, the controllable propagation of the CAi beam is also demonstrated in our investigation. The Airy beam in atomic vapors broadens the application potential of atomic vapors and inspires new ideas in research associated with atomic vapors.

**Acknowledgements** Z. Wu acknowledges the Key University Science Research Project of Henan Province (Grant No. 17A140003), Postdoctoral Research Sponsorship (Grant No. 190308), and the Natural Science Foundation of Shaanxi Province (Grant No. 2016JM1006). H. Guo acknowledges the Postdoctoral Research Sponsorship in Henan Province (Grant No. 2014035) and Postdoctoral Research Sponsorship (No. BH2014033). Y. Gu acknowledges the Science and Technology Department of Henan Province (Grant No. 144300510018).

## Appendix A The density matrix equations

We begin our analysis by considering propagation of the probe field in the Λ-type three-level atomic system, and it is described by the density-matrix equation of motion

$$\dot{\rho} = -\frac{\mathrm{i}}{\hbar}[H,\rho] - \frac{1}{2}\{\Gamma,\rho\},$$

with

$$H = \hbar(\omega_{21}|1\rangle\langle 1| + \omega_{23}|2\rangle\langle 2|) + (\Omega_p|1\rangle\langle 2| + \Omega_c|2\rangle\langle 3| + \mathrm{H.c.})$$

as the Hamiltonian of the atomic system. Considering the time-dependent Schrodinger equation, using a perturbation expansion and rotating wave approximation, we can obtain a series of density matrix equations as follows [20, 21]:

$$\frac{\partial}{\partial t}\sigma_{11} = -\Gamma_{11}\sigma_{11} + \mathrm{i}(\Omega_p\sigma_{21} - \Omega_p^*\sigma_{12}), \tag{A1}$$

$$\frac{\partial}{\partial t}\sigma_{21} = -(\Gamma_{21} + \mathrm{i}\Delta_p)\sigma_{21} - \mathrm{i}\Omega_p(\sigma_{22} - \sigma_{11}) + \mathrm{i}\Omega_c\sigma_{31}, \tag{A2}$$

$$\frac{\partial}{\partial t}\sigma_{22} = -\Gamma_{22}\sigma_{22} + \mathrm{i}[(\Omega_p^*\sigma_{21} - \Omega_p\sigma_{12}) + \Omega_c^*(\sigma_{32} - \sigma_{23})], \tag{A3}$$

$$\frac{\partial}{\partial t}\sigma_{31} = -[\Gamma_{31} + \mathrm{i}(\Delta_p - \Delta_c)]\sigma_{31} + \mathrm{i}\Omega_p^*\sigma_{32} + \mathrm{i}\Omega_c\sigma_{21}, \tag{A4}$$

$$\frac{\partial}{\partial t}\sigma_{32} = -(\Gamma_{32} - \mathrm{i}\Delta_c)\sigma_{32} - \mathrm{i}\Omega_c^*(\sigma_{22} - \sigma_{33}) + \mathrm{i}\Omega_p\sigma_{31}, \tag{A5}$$

$$\frac{\partial}{\partial t}\sigma_{33} = -\Gamma_{33}\sigma_{33} + \mathrm{i}(\Omega_c^*\sigma_{32} - G_c\sigma_{23}). \tag{A6}$$

## Appendix B Derivation of the susceptibility

We display the detailed derivation process of $-\frac{\eta}{K^2}\frac{|\Omega_c|^2}{d_3}$ using the *dressed perturbation chain method* [22], which involves the perturbation chain [23] and coupling equations together.

First, a ground state particle $\sigma_{11}^{(0)}$ absorbs a probe photon $p$ and transits to $\sigma_{\Omega_c\pm1}^{(1)}$, the dressed state of $\sigma_{21}^{(1)}$ ($\sigma_{11}^{(0)} \xrightarrow{\Omega_p} \sigma_{\Omega_c\pm1}^{(1)}$). With the weak-field and steady-state approximations, the coupling equations can be obtained from Eqs. (A2) and (A4):

$$0 = -(\Gamma_{21} + \mathrm{i}\Delta_p)\sigma_{21} - \mathrm{i}\Omega_p(\sigma_{22} - \sigma_{11}) + \mathrm{i}\Omega_c\sigma_{31},$$

$$0 = -[\Gamma_{31} + \mathrm{i}(\Delta_p - \Delta_c)]\sigma_{31} + \mathrm{i}\Omega_p^*\sigma_{32} + \mathrm{i}\Omega_c\sigma_{21},$$

which gives

$$\sigma_{G_c\pm0}^{(1)} = \frac{\mathrm{i}\Omega_p}{\Gamma_{21} + \mathrm{i}\Delta_p + \frac{|\Omega_c|^2}{\Gamma_{31} + \mathrm{i}(\Delta_p - \Delta_c)}}\sigma_{11}^{(0)}. \tag{B1}$$

Second, the particle absorbs a coupling photon $c$ and transits to the state $\sigma_{31}^{(2)}$ ($\sigma_{G_c\pm1}^{(1)} \xrightarrow{\Omega_c} \sigma_{31}^{(2)}$). From Eqs. (A4) and (A5) as well as the approximations used in the first step, we get the coupling equations

$$0 = -[\Gamma_{31} + \mathrm{i}(\Delta_p - \Delta_c)]\sigma_{31} + \mathrm{i}\Omega_p^*\sigma_{32} + \mathrm{i}\Omega_c\sigma_{21},$$

$$0 = -(\Gamma_{32} - \mathrm{i}\Delta_c)\sigma_{32} - \mathrm{i}\Omega_c^*(\sigma_{22} - \sigma_{33}) + \mathrm{i}\Omega_p\sigma_{31},$$

which gives

$$\sigma_{31}^{(2)} = \frac{\mathrm{i}\Omega_c}{\Gamma_{31} + \mathrm{i}(\Delta_p - \Delta_c) + \frac{|\Omega_p|^2}{\Gamma_{32} - \mathrm{i}\Delta_c}}\sigma_{G_c\pm0}^{(1)}. \tag{B2}$$

Third, the stimulated atom transits back to state $\sigma_{21}$ and emits a coupling photon $c^*$ ($\sigma_{31}^{(2)} \xrightarrow{\Omega_c^*} \sigma_{\Omega_c\pm1}^{(3)}$). Combining Eqs. (A1) and (A2), we get the coupling equations

$$0 = -\Gamma_{11}\sigma_{11} + \mathrm{i}(\Omega_p\sigma_{21} - \Omega_p^*\sigma_{12}),$$

$$0 = -(\Gamma_{21} + \mathrm{i}\Delta_p)\sigma_{21} - \mathrm{i}\Omega_p(\sigma_{22} - \sigma_{11}) + \mathrm{i}\Omega_c\sigma_{31},$$

and the corresponding solution

$$\sigma_{\Omega_c\pm0}^{(3)}=\frac{\mathrm{i}\Omega_c}{\Gamma_{21}+\mathrm{i}\Delta_p+\frac{|\Omega_p|^2}{\Gamma_{11}}}\sigma_{31}^{(2)}. \tag{B3}$$

Combining Eqs. (B1)–(B3) and considering the assumption $\sigma_{11}^{(0)}\approx 1$ as well as the relations $P=N\mu_{21}\sigma_{\Omega_c\pm0}^{(3)}=\varepsilon_0\chi^{(3)}|E_c|^2E_c$, we finally obtain the expression for the susceptibility:

$$\chi^{(3)}|E_c|^2=-\frac{\mathrm{i}N\mu_{21}^2}{\hbar\varepsilon_0}\frac{1}{\left[\Gamma_{21}+\mathrm{i}\Delta_p+\frac{|\Omega_c|^2}{\Gamma_{31}+\mathrm{i}(\Delta_p-\Delta_c)}+\frac{|\Omega_p|^2}{\Gamma_{11}}\right]^2}\frac{|\Omega_c|^2}{\Gamma_{31}+\mathrm{i}(\Delta_p-\Delta_c)+\frac{|\Omega_p|^2}{\Gamma_{32}-\mathrm{i}\Delta_c}}. \tag{B4}$$

## References


1. G. A. Siviloglou and D. N. Christodoulides, Accelerating finite energy Airy beams, *Opt. Lett.* 32(8), 979 (2007)
2. G. A. Siviloglou, J. Broky, A. Dogariu, and D. N. Christodoulides, Observation of accelerating Airy beams, *Phys. Rev. Lett.* 99(21), 213901 (2007)
3. J. Broky, G. A. Siviloglou, A. Dogariu, and D. N. Christodoulides, Self-healing properties of optical Airy beams, *Opt. Express* 16(17), 12880 (2008)
4. M. V. Berry and N. L. Balazs, Nonspreading wave packets, *Am. J. Phys.* 47(3), 264 (1979)
5. Y. Q. Zhang, M. R. Belić, Z. K. Wu, H. B. Zheng, K. Q. Lu, Y. Y. Li, and Y. P. Zhang, Soliton pair generation in the interactions of Airy and nonlinear accelerating beams, *Opt. Lett.* 38(22), 4585 (2013)
6. Z. K. Wu, P. Li, and Y. Z. Gu, Propagation dynamics of finite-energy Airy beams in nonlocal nonlinear media, *Front. Phys.* 12(5), 124203 (2017)
7. Y. Q. Zhang, M. R. Belić, H. B. Zheng, H. X. Chen, C. B. Li, Y. Y. Li, and Y. P. Zhang, Interactions of Airy beams, nonlinear accelerating beams, and induced solitons in Kerr and saturable nonlinear media, *Opt. Express* 22(6), 7160 (2014)
8. C. D. Chen, B. Chen, X. Peng, and D. M. Deng, Propagation of Airy–Gaussian beam in Kerr medium, *J. Opt.* 17(3), 035504 (2015)
9. Z. K. Wu and Y. Z. Gu, Laguerre–Gaussian, Hermite–Gaussian, Bessel–Gaussian, and Finite-Energy Airy beams carrying orbital angular momentum in strongly nonlocal nonlinear media, *J. Phys. Soc. Jpn.* 85(12), 124402 (2016)
10. B. Chen, C. D. Chen, X. Peng, Y. L. Peng, M. L. Zhou, D. M. Deng, and H. Guo, Evolution of the ring Airy Gaussian beams with a spiral phase in the Kerr medium, *J. Opt.* 18(5), 055504 (2016)
11. F. Zhuang, J. Shen, X. Du, and D. Zhao, Propagation and modulation of Airy beams through a four-level electromagnetic induced transparency atomic vapor, *Opt. Lett.* 37(15), 3054 (2012)
12. C. Hang and G. Huang, Slow-light Airy wave packets and their active control via electromagnetically induced transparency, *Phys. Rev. A* 88(1), 013825 (2013)
13. F. J. Ye, L. Y. Zhang, F. R. Wang, Y. M. Yang, Y. Yu, J. Liu, D. Wei, P. Zhang, H. Gao, and F. L. Li, Propagation of Airy beams in a close-Λ electromagnetically induced transparency system, *Opt. Commun.* 345, 129 (2015)
14. Z. K. Wu, S. Wang, W. F. Hu, and Y. Z. Gu, Dynamics of finite energy airy beams carrying orbital angular momentum in multilevel atomic vapors, *J. Phys. Soc. Jpn.* 85(10), 104302 (2016)
15. S. Tanev and D. Pushkarov, Solitary wave propagation and bistability in the normal dispersion region of highly nonlinear optical fibers and waveguides, *Opt. Commun.* 141(5–6), 322 (1997)
16. Z. K. Wu, Y. Q. Zhang, C. Z. Yuan, F. Wen, H. B. Zheng, Y. P. Zhang, and M. Xiao, Cubic-quintic condensate solitons in four-wave mixing, *Phys. Rev. A* 88(6), 063828 (2013)
17. Z. K. Wu, K. G. Chang, Y. Hu, Y. Z. Zhang, Z. H. Jiang, and Y. P. Zhang, Modulation of four-wave mixing via photonic band gap, *Front. Phys.* 9(5), 665 (2014)
18. H. Michinel, M. J. Paz-Alonso, and V. M. Perez-Garcia, Turning light into a liquid via atomic coherence, *Phys. Rev. Lett.* 96(2), 023903 (2006)
19. D. E. Edmundson and R. H. Enns, Particle-like nature of colliding three-dimensional optical solitons, *Phys. Rev. A* 51(3), 2491 (1995)
20. A. S. Desyatnikov, Y. S. Kivshar, and L. Torner, Optical vortices and vortex solitons, *Prog. Opt.* 47, 291 (2005)
21. Y. P. Zhang, Z. G. Wang, Z. Q. Nie, C. B. Li, H. X. Chen, K. Q. Lu, and M. Xiao, Four-wave mixing dipole soliton in laser-induced atomic gratings, *Phys. Rev. Lett.* 106(9), 093904 (2011)
22. Y. P. Zhang, Z. Q. Nie, and M. Xiao, Coherent Control of Four-Wave Mixing, Heidelberg: Springer, 2010
23. S. E. Harris, Electromagnetically induced transparency, *Phys. Today* 50(7), 36 (1997)
24. I. Chremmos, P. Zhang, J. Prakash, N. K. Efremidis, D. N. Christodoulides, and Z. Chen, Fourier-space generation of abruptly autofocusing beams and optical bottle beams, *Opt. Lett.* 36(18), 3675 (2011)
25. P. Panagiotopoulos, D. G. Papazoglou, A. Couairon, and S. Tzortzakis, Sharply autofocused ring-Airy beams transforming into non-linear intense light bullets, *Nat. Commun.* 4, 2622 (2013)

26. J. Sun, Z. C. Zuo, X. Mi, Z. H. Yu, Q. Jiang, Y. B. Wang, L. A. Wu, and P. M. Fu, Two-photon resonant four-wave mixing in a dressed atomic system, *Phys. Rev. A* 70(5), 053820 (2004)

27. H. Li, V. A. Sautenkov, Y. V. Rostovtsev, G. R. Welch, P. R. Hemmer, and M. O. Scully, Electromagnetically induced transparency controlled by a microwave field, *Phys. Rev. A* 80(2), 023820 (2009)

28. Z. Q. Nie, H. B. Zheng, P. Z. Li, Y. M. Yang, Y. P. Zhang, and M. Xiao, Interacting multiwave mixing in a five-level atomic system, *Phys. Rev. A* 77(6), 063829 (2008)

29. P. M. Fu, X. Mi, Z. H. Yu, Q. Jiang, Y. P. Zhang, and X. F. Li, Ultrafast modulation spectroscopy in a cascade three-level system, *Phys. Rev. A* 52(6), 4867 (1995)